A Comparison of Methods for Astrometric Measurements of Close Double Stars

Alex Cherney
Melbourne, Australia
alex@terrastro.com

Abstract: Off-the-shelf equipment – an 8-inch Schmidt-Cassegrain telescope and a DSLR camera - were used for observations of 18 double stars with separation in the 0.5 – 11" range.

All 18 double stars were measured with the Speckle Interferometry method. 8 double stars were also measured with the Lucky Imaging method and 5 – with the Video Drift Method. The results obtained with each method were compared with computed ephemerides from published orbits and latest precise observations.

Speckle interferometry measurements of double stars wider than 1" produced the average O-C residuals of 0.52º PA and 0.04" separation. For the Lucky Imaging method, the average residuals were 0.9º and 0.03". For the pairs wider than 4.3" Video Drift method was applicable and the residuals were 0.46º and 0.06". A potential error in the Sixth Orbit Catalog for HDO 182 (λ Scl) Grade 5 orbit was identified.

A brief historic background of double star research, methods of measurement and results are presented. Additionally, the quantitative assessment of methods with error analysis is performed.

Introduction

A variety of methods for measuring separations and position angles of double stars are readily available to the amateur astronomy community. These methods range from a micrometer eyepiece for visual observations to Speckle Interferometry, using high-speed digital video cameras for accurate diffraction-limited measurements (Argyle 2012). The main goal of this research project is to assess and compare methods for astrometric measurements of relatively close visual double stars, attainable with modest optical equipment and off-the-shelf digital video cameras.

The precision of double star measurements with a video camera depends on a number of factors, such as the resolving power and optical quality of the telescope, stability of the tracking mount, resolution of the CCD or CMOS detector and, and last but not least, distortions introduced by Earth's atmosphere. Optical, mechanical and electronic factors can be addressed by selecting the appropriate equipment, but unfortunately, favourable atmospheric seeing cannot be simply "ordered" and quite often the observations have to be performed in rather poor seeing conditions.

Speckle Interferometry (Labeyrie 1970) and Lucky Imaging (Boffin et al. 2016) methods overcome the seeing effects by using short exposures and can achieve accurate results with smaller aperture telescopes, approaching the theoretical resolution limits.

A large number of amateur astronomers own reflector telescopes on Altitude-Azimuth mounts, some with considerable resolving power (apertures of 20 inches and above). Video Drift method (Nugent & Iverson 2011) uses multiple position measurements to produce accurate results without expensive Equatorial mounts, required to support larger telescopes.

The goal of this research project is to assess double star measurement methods available to amateur astronomers with modest commercially available equipment – a telescope with an 8-inch aperture and a DSLR camera, which can also be used for day-time photography of cats, dogs and other objects of interest.

The observations were made with 8" Schmidt-Cassegrain telescope at 37.98° S latitude, 145.06° E longitude, Melbourne, Australia

History of double star observations

The term "double star" was first mentioned by Ptolemy when he described v1 and v2 Sagittarii in his star

catalog from 2nd century AD (Heintz 1978). Using modern terminology, we would call it an "optical double" because v1 and v2 Sagittarii are not gravitationally bound and have an appearance of a double star due to a coincidental line of sight alignment, as viewed from Earth.

Until late 18th century the common assumption amongst astronomers was that double stars were located close to each other in the sky by chance. That changed however, when John Mitchell used mathematical statistics and argued (Mitchell 1767) that stars did not follow random distribution on the celestial sphere and there were a lot more stars grouped in some parts of the sky, compared to the others due to some general law (perhaps gravity). Soon after Mitchell's paper, W. Herschel began to study double stars with his powerful reflecting telescopes. Over the course of 25 years he noticed a change of position in some pairs of stars and proposed that these were due to orbital motions.

In the 19th century the studies of double stars became more systematic. Wilhelm Struve used a micrometer to discover and reobserve more than 3,000 double stars (Heintz 1978). The results of his work – a number of double star catalogs – are still used for orbital calculations of long term double stars.

Application of plate photography and, later high-speed CCD imaging, revolutionised the field of double star research in the 20th century. It allowed astronomers to observe visual doubles with milli-arcsecond precision using lucky imaging and speckle interferometry and utilise innovative observational methods of double star research, such as spectroscopy and precise photometry.

Numerous catalogs with double star observations and measurements have been published since the 18th century. The United States Naval Observatory (USNO) produces the most current and widely used Washington Double Star (WDS) catalog. The measures in the catalog have been "collected, collated, and maintained since the early 1960's". As of March 24, 2018 there are 142,563 systems in the catalog (wds_web).

Telescope Resolution

Light from the stars and other celestial objects is diffracted as it passes through a circular aperture of an optical telescope. As the result of the diffraction, the light emitted by a point-like source (a star) forms a bright central disk (the Airy disk) surrounded by the series of light and dark concentric rings (Airy pattern) (Argyle 2012). The angular diameter (in radians) of the central disk, D_{Airy}, for the monochromatic point-like source of light with wavelength λ passing through an unobstructed circular aperture with the diameter D and the telescope focal length f can be approximated as

$$D_{Airy} = \frac{2.44\lambda f}{D} \quad \text{rad} \qquad [1]$$

The image of two stars is comprised of two diffraction patterns and the individual star images are considered to be just resolved, under idealized atmospheric conditions, if the center of the Airy disk of the first star coincides with the first dark ring of the second star's Airy pattern. This telescope angular resolution limit θ_{res} is called Rayleigh criterion and can be approximated as

$$\theta_{res} = \frac{1.22\lambda}{D} \quad \text{rad} \qquad [2]$$

For the 8" Schmidt-Cassegrain telescope with the 34% central obstruction and a broadband source of light, equation [2] provides a reasonable resolution estimate. Considering λ = 550 nm, the resolution limit is:

$$\theta_{res} = (1.22)\frac{\left(5.5\times10^{-7}\,\text{m}\right)}{0.2\,\text{m}} \approx 3.36\times10^{-6}\ \text{rad} \approx 0.7"$$

Atmospheric seeing effects

Using a simplified view, atmospheric turbulence causes dynamic variations in the distribution of cold and warm cells of air. The differences in temperature between the air cells result in the localized differences in pressure and contribute to the differential refractive index in the neighboring cells. This differential refraction distorts the plane wave fronts originating from a point light source in the sky (Figure 1). Such distortion is often referred to as "λ = 550 atmospheric seeing".

This distortion causes twinkling of stars when we

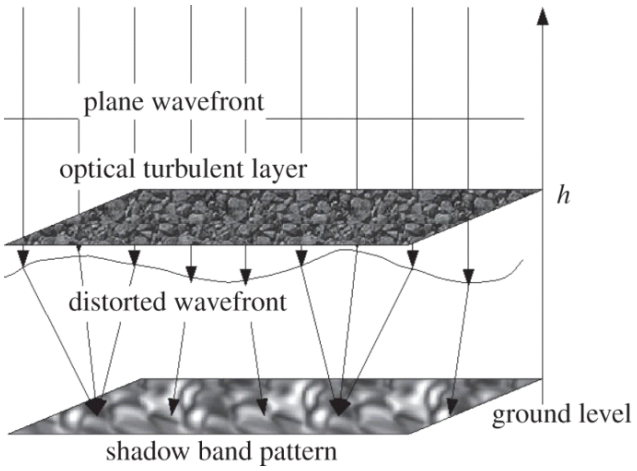

Figure 1. Propagation of light through a layer of atmospheric turbulence. Image by Sofieva et al. 2013)

look at them from Earth and also blurs the image at the telescope eyepiece or the CCD/CMOS camera. Atmospheric seeing is the most significant factor limiting resolution for all but the smallest ground-based telescopes.

The properties of the atmospheric seeing are defined by two main parameters (Boffin et al. 2016):

The atmospheric spatial coherence parameter, r_0, (Fried parameter), which defines the diameter of an average air cell.

The atmospheric coherence time, t_0, representing the interval over which the air cell of diameter r_0 affects the plane wavefront.

The Fried parameter r_0 is proportionate to the wavelength λ of the incoming light and can be expressed as:

$$r_0 = 1.009D\left(\frac{\lambda}{\theta_{seeing}}\right)^{\frac{6}{5}} \quad [3]$$

where θ_{seeing} is the full width half maximum (FWHM) diameter of the atmospheric seeing disc in radians and D is the telescope aperture diameter in metres (Argyle 2012). θ_{seeing} also increases proportionately to the zenith angle (the angle between the star and the local zenith) due to larger airmass.

The average atmospheric seeing FWHM recorded during the observing runs at the author's principal observing site in the southeastern part of Melbourne, Victoria, Australia was measured around 2". For the 8" telescope and λ = 550 nm, the Fried parameter, r_0, is approximately 4cm.

Atmospheric dispersion

Earth's atmosphere acts on the incoming light like a prism and refracts wavelengths differently, bending blue light more than red. Such refraction affects the shape and the measured position of a star.

For a double star with O5 and M5-class components, observed at 45º zenith angle (the angle between the star and the local zenith) the difference in separation is around 0.1" for the V-band filter (Rutkowski & Waniak 2005). Specialized dispersion correction devices can be employed to correct the dispersion, such as counter-rotating Risley prisms (Genet et al. 2015).

In order to minimize the atmospheric dispersion, the double stars with small difference in stellar classes were selected for observations at low zenith angles (less than 35º).

2. Equipment

The equipment used for observations in this research project included Celestron EdgeHD 800 Schmidt -Cassegrain telescope on a computer-controlled Losmandy G11 tracking German Equatorial mount and Canon 6D DSLR camera with Televue 4x Powermate image amplifier. Figure 2 shows the equipment setup and ready for an observing run.

Figure *2. Celestron Edge HD 800 with Canon 6D on Losmandy G11 mount*

Canon 6D DSLR Camera

Canon 6D is a single-shot colour camera equipped with 35.8 x 23.9 CMOS detector and DIGIC 5+ image processor. The full resolution is 5472 x 3648 pixels and the pixel size is 6.54 microns. The camera has been modified to run open source Magic Lantern software (magic_lantern_web), which allows it to record video in RAW format using the central section of the detector without scaling the image, making it particularly useful for the astrometry.

The full frame image is used to confirm the telescope pointing and to determine the image scale and camera orientation using astrometric plate-solving technique.

The ISO sensitivity (gain) range is 100 – 102400. The camera is equipped with a thermo-electric cooler, which is unregulated and achieves detector temperature of around 18º C below the temperature of ambient air.

Being a single-shot colour camera, Canon 6D includes red, green and blue colour filters located above the detector and arranged in a "Bayer" matrix. It facilitates the capture all colour information in one image but, depending on the colour, only one or two out of four pixels in each image contain signal from the specific colour. Moreover, the colour filters differ in the

(Text continues on page 655)

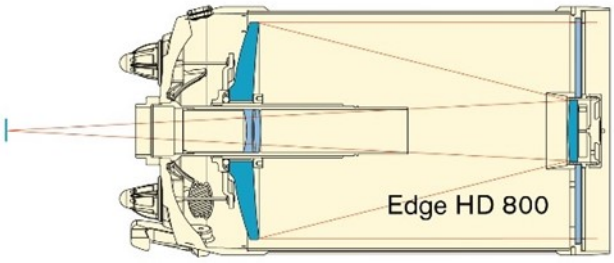

Figure 3.. Celestron Edge HD 800 telescope. (image by Celestron_EdgeHD_web)

amount of light they let through.

These limitations may potentially affect the determination of the precise position of a star, based on a point spread function fitting. In order to mitigate that effect in speckle interferometry measurements, a Gaussian lowpass spatial filter is used, and multiple images are averaged in the lucky imaging method. For the video drift method, a different technique is used and a monochrome image is constructed from the red, green and blue channels without debayering, resulting in half effective resolution.

Celestron Edge HD 800 corrected Schmidt-Cassegrain telescope and image amplifier

Celestron Edge HD 800 (Figure 3) is a Schmidt-Cassegrain telescope with aperture of 203mm and focal ratio of f/10 (Celestron_EdgeHD_web). The secondary obstruction is 68.6mm or 34%. The telescope is fitted with an optical corrector which provides a highly corrected field over 42mm diameter.

Televue Powermate 4x image amplifier was used to achieve the f/ratio of f/40 required to observe close double stars using speckle interferometry and lucky imaging methods.

Losmandy G11 German Equatorial tracking mount

Losmandy G11 computerised German Equatorial mount tracks the celestial objects and allows for computer control using ASCOM standard protocol (ASCOM_web) and permanent Periodic Error Correction (PEC). The mount was carefully polar-aligned using drift-alignment technique and periodic error was measured and corrected for, in order to keep the observed double stars in the centre of the field of view.

The mount provides excellent support for the Celestron EdgeHD 800 telescope and Canon6D camera and autoguiding is not required for the short exposures used in the observations.

3. Observational workflow

Limiting Visual Magnitude

Prior to the selection of observational targets, a number of single stars were observed in order to determine the limiting visual stellar magnitude resulting in an acceptable signal-to-noise ratio for the longest exposure limit set at 30ms.

Image Scale and Camera Orientation

In order to measure double star separation and position angle parameters it is necessary to determine the image scale in arcseconds per pixel and camera orientation in relation to North and East. To achieve statistically robust image scale and camera orientation values, the following two methods were applied:

1. Astrometric plate solving using PlateSolve2 software, developed by David Rowe (planewave_web). This method measures image scale and camera orientation with very low error values (typical errors were less than 1%).
2. Video Drift method automatically determines the plate scale and camera orientation using known Declination of the double star and precise timing from the video sequence.

The camera remained in the same position for the duration of several observing runs unless the telescope was moved into storage. Average camera orientation angle and image scale values were calculated and used for a series of observing runs when the telescope was left in the field and not disturbed.

Image Acquisition and processing workflow

Telescope pointing and tracking were performed using Sequence Generator Pro software (sgpro_web). This software provides integration with PlateSolve2 for automatic determination and adjustment of the telescope pointing position. It also keeps the log of observed targets with timestamps.

Before starting the observation of a specific double star, a 30-second exposure was taken by Sequence Generator Pro software, utilising the full frame of Canon 6D (5472 x 3648 pixels). The image centre coordinates were determined using astrometric plate solving and a slew command issued to move the telescope to the correct position if required. The same data used for telescope pointing adjustment was used for astrometric determination of the image scale and camera orientation.

Video recording. For each target, the star was centered in the Canon 6D field of view and 864 x 864 pixels video sequence was recorded using the central section of the detector. After recording of the tracked sequences was complete, the target was placed at the edge of the frame, video recording started and the telescope drive turned off. When the target drifted off the opposite edge of the frame, the telescope clock drive was turned back on. The aforementioned process was repeated twice, resulting in two tracked sequences and two video drift sequences.

During the first three observing runs the tracked sequence duration was just over 70 seconds, resulting in approx. 2,000 video frames. After the initial data reduction, it was determined that longer runs of around 180 seconds would produce 5,000 frames and allow for improved statistical analysis. Therefore, during last three observing runs longer 3-minute tracked sequences were recorded.

For each reference star, two 3-minute long tracked video sequences were recorded, resulting in approx. 5,000 frames in each sequence.

Image Conversion. The first step was to convert RAW video images produced by Magic Lantern software in MLV container format to individual Adobe DNG files. MLVMystic software program (mlvmystic_web) was used for this conversion. Then the DNG files were visually examined, first and last few hundred frames deleted to avoid any distortions due to telescope vibrations when the video recording was triggered manually. Selected DNG files were converted to monochrome FITS files in PixInsight software – without debayering for Speckle Interferometry and Lucky Imaging; and using SuperPixel method (2x2 binning) for the Video Drift method.

Image pre-processing was done in Speckle Toolbox. The FITS images were grouped into FITS cubes, with 1,000 images per cube for data reduction in Speckle Toolbox (Speckle Interferometry) and REDUC (Lucky Imaging). An observation would result in 8 cubes per double or reference star during the first three observing runs and 10 FITS cubes during the last three runs. For the Video Drift method, the converted FITS files were sorted into folders, named in accordance with the double star designation.

Data Reduction. 8 – 10 FITS cubes, pre-processed in the previous step were analyzed in Speckle Toolbox and REDUC programs (described in section 4). Average results and standard deviation values were computed in Microsoft Excel for each observed double star. The data reduction results were saved as tables for each of the measurement methods.

Drift videos, converted to 2 x 2-binned FITS sequences were reduced in Tangra3 program and measured positions saved in a text file. The drift data was pasted into VidPro Excel spreadsheet and analysed.

4. Double Star Measurements

Speckle Interferometry

Labeyrie (1970) used a laser beam to simulate a star and a silicone-sprayed glass plate, placed in front of the telescope, to simulate the atmsopheric seeing. He then developed a method for recovering the high-resolution structure from the distorted image by applying a Fourier transform to the series of speckle images and obtaining the sum of their power spectra.

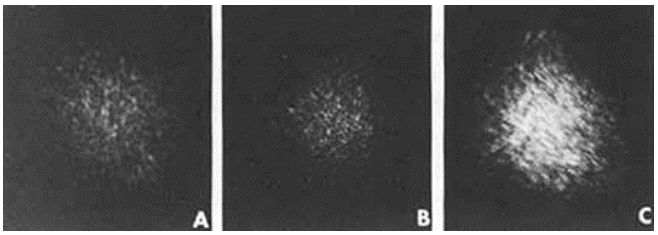

Figure 4. Speckle photographs of Betelgeuse (A), Bellatrix (B) and a close double star Capella obtained with the Kitt Peak 4-m telescope. Image by history_nasa_web

The dynamic atmospheric cells are responsible for the degradation of the telescopic image, if the image integration time is greater than atmospheric coherence time t_o (the average lifetime of the atmospheric cell). However, if the image integration time is less than the average lifetime of the atmospheric cell then the image of a star will be a combination of small spots, called "speckles" caused by the constructive and destructive interference of light, as it passes through the atmospheric cells (Figure 4).

Such speckle image preserves the diffraction limited information, which is considerably better than the size of the atmospheric seeing disk for all but the smallest telescopes.

If two components of a double star are close enough in the sky then their light passes through the same pattern of refractive cells in the atmsophere (isoplanatic patch). As the result, the same atmospheric point spread function applies to both double star components or, in more poetic terms – the two stars "twinkle" together. The maximum separation for a double star to be in the same isoplanatic patch under average atmospheric seeing is around 5" – 7". The average time for the isoplanatic patch to exhibit a significant change depends more on the wind speed than the movements of the individual air cells and is typically in the order of 10ms (Boffin et al. 2016).

The number of speckles N in the image, for the telescope with aperture D and the Fried parameter r_o can be estimated as:

$$N = \frac{D^2}{r_o^2} \qquad [4]$$

For the Celestron EdgeHD 800 telescope used for observations D = 0.2 m and r_o = 0.04 m the number of speckles N present in the image is expected to be around 25.

Figure 5 shows a magnified image with a resem-

Figure 5. 0.004 second exposure of a reference star (Fomalhaut) with 0.2m telescope

blance of the speckle pattern, in a 0.004s exposure of a reference star (Fomalhaut) obtained during an observing run on November 2, 2017. The image scale of 0.18" per pixel is too large and not all individual speckles are resolved, unlike in the image obtained with 4-meter Kitt Peak telescope (Figure 4).

Speckle data reduction was performed in Speckle Toolbox (ST) software written by David Rowe and distributed free of charge (Harshaw et al., 2017).

The data reduction in ST requires the steps outlined below.

FITS cubes pre-processing

A FITS cube with a double or reference star is loaded and a Fast Fourier Transform (FFT) of every image in the cube is computed. Subsequently all transforms are averaged and a Power Spectral Density (PSD) file is produced. The PSD file is considerably smaller in size than the FITS cube -– 1Mb vs 500MB for 1,000 image cube. ST offers a convenient feature to preprocess multiple FITS cubes in a batch.

Speckle Reduction

The double star and reference PSD files, preprocessed in the step 1, are opened and appropriate values for Low-Pass and High-Pass dimensional filters are selected.

The reference PSD is a power spectral density file of a reference single star located near the observed double star in the sky. It should be recorded using a very short exposure time (ideally less than 5 ms). It is used to sharpen the double star image by removing the effects of the telescope central obstruction and optical aberrations as well as most of the atmospheric dispersion. In ST the deconvolution process divides the double star PSD by the reference PSD (Harshaw et al. 2017)

$$\langle O \rangle = \frac{\langle I \rangle}{\langle T \rangle} \qquad [5]$$

where $\langle I \rangle$, $\langle T \rangle$, and $\langle O \rangle$, are the averages of Fourier transforms of the double star image, the reference star (representing telescope and atmospheric aberrations) and the deconvolved image, respectively. Subsequent inverse Fourier Transform of $\langle O \rangle$ produces the autocorrelation which can be measured by the ST astrometry tool.

The *Low-Pass Gaussian filter* removes the noise originating from the in-camera electronic processing circuits, sky background and photon shot noise. For the images taken with Canon 6D one-shot colour camera, the Gaussian Low-Pass filter also addresses the difference in signal passing through the individual colour filters of the Bayer matrix.

The value for the Low-Pass filter radius f_c (in pixels) should be set with a cut-off frequency slightly wider than the following value (Harshaw et al. 2017):

$$f_c = \frac{hN}{2.44 \lambda F/D} \qquad [6]$$

where λ is the wavelentgh, h is the pixel dimension and F/D is the effective focal ratio of the optical system.

For the Celestron EdgeHD 800 with 4x image amplifier, Canon 6D camera with 6.55 micron pixels, λ = 550 nm, N = 512, and f_c = 62 pixels.

Setting the Low-Pass filter value to a slightly wider value of 70 pixels empirically produced best results.

The purpose of the *High-Pass Gaussian filter* is to eliminate the effects of optical aberrations and atmospheric seeing by cutting off the wide end of the point-spread function.

The value of this filter is adjusted by inspecting the PSD image and making sure that it removes the bright central peak but does not cut off useful signal by extending beyond the zero-order fringe pattern in the PSD image (Figure 6).

During the first two observing runs the reference star images were not taken and a larger value for the Low-Pass filter was used instead. Additionally for very close double stars (separation less than 1"), the deconvolution using a reference star did not result in a resolvable image. For those double stars a symmetrised point spread function was subtracted from the image, leaving non-symmetrical part only (Harshaw et al. 2017). Reasonable results were achieved using this method for very close doubles.

Astrometry Tool

After selecting the appropriate values for the filters, ST performs another Fast Fourier Transform and produces an autocorellogram, which can be directly measured with the ST Astrometry Tool.

Figure 6. Gaussian high pass filter examples. Left - too wide (cuts off the central peak and the fringe pattern), centre - set correctly, right – too narrow (allows the central peak to be seen). Image adapted from Harsahw et al. (2017)

In the ST *Astrometry Tool*, the scale calibration values – plate scale in arcseconds per pixel and camera orientation in degrees – are entered. The measuring circle is placed around the secondary component (Figure 7). A right-click on the circle opens the context menu and "Set Target Location" is selected. Then ST computes the accurate position of the secondary component in relation to the centre, based on the centroid value. The ST Astrometry tool provides an automatic selection of the target location, but it may not always work depending on other bright parts of the image. In that case the measuring circle is placed manually.

The separation is converted from pixels to arcseconds by ST automatically, based on the plate scale. The position angle however, carries the 180° uncertainty and ST uses known information about the double star, supplied as an input parameter in order to resolve this ambiguity. The measurement results are then written to a comma-separated text file for further statistical analysis.

ST allows for semi-automatic processing of PSD files and takes a text file with input parameters to make the reduction of large number of FITS cubes less laborious.

Lucky Imaging

The lucky imaging method, like the Speckle Interferometry method, requires exposure times comparable with the atmospheric coherence time t_o, however instead of computing a power spectrum density over all exposures, the lucky imaging method uses a selection process to include only those images that match quality criteria. Typically, around 1-5% of the images are included based on the point spread function fitting.

The lucky imaging data reduction is performed in REDUC software written by Florent Losse and distributed free of charge (Harshaw et al. 2017).

The data reduction in REDUC is performed using "Easy Lucky Imaging" process. After selecting rough positions for primary and secondary double star components, REDUC uses point spread function fitting to select, align and stack the best frames, producing an image that can be more reliably measured than individual frames.

Figure 8 shows three images from an observation sequence for WDS22266-1645 double star. The typical unlucky and lucky frames were taken less than 0.2 s apart (images A and B). Image C is an aligned stack of 55 lucky images as selected by the Easy Lucky Imaging algorithm in REDUC. It demonstrates that stacking makes it possible to determine the peaks with reasonable accuracy. For close doubles, the center peaks were determined using SURFACE algorithm, which takes into account an empirical model of the atmospheric point-spread function. Pairs wider than 3" were processed using AutoReduc method, which measures posi-

(Text continues on page 659)

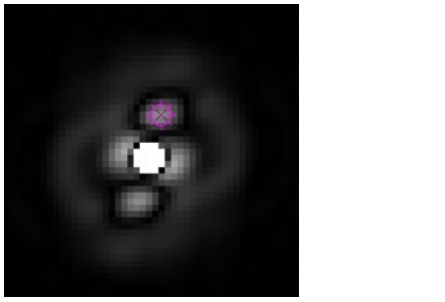

Figure 7. Autocorellogram for WDS22266-1645 with automatic peak selection circle placed by ST. Separation 1.3"

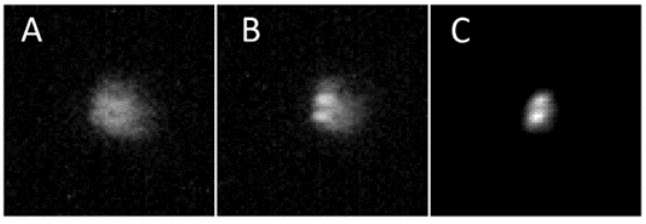

Figure 8. Magnified images of WDS22266-1645 (Exposure: 30ms, Separation 1.3"). A - Unlucky image, B – Lucky image, C – Aligned and stacked series of best 55 lucky images.

tions of each frame in the "lucky" set and calculates an average value.

Video Drift

Tangra astrometric video analysis software (tangra_web) was used to reduce 840x840 pixels video drift sequences. Tangra is a software program with open source code, developed and maintained by Hristo Pavlov. It is designed for astronomical video observations of asteroid occulations and can track and perform aperture photometry of stars, as they drift across the frame. Thanks to the program's open source code, the author of this paper was able to modify the program code and append (*x,y*) positions of the measured stars to the exported light curve data, making it suitable for double star video drift measurement method.

Tangra analyses the individual FITS files from a folder, tracks the drifting stars using Point Spread Function fitting and records their (*x,y*) positions. The values are recorded with 0.1-pixel precision. After successful tracking of the video frames, the series of positions are saved into a text file for further analysis in the VidPro Excel spreadsheet.

The VidPro Excel spreadsheet, originally developed by Nugent & Iverson (2011), was modified to accept the output from Tangra software. The orientation of the camera detector and the drift angle are determined for each video using least squares regression fitting from all measured (*x,y*) coordinate pairs. The position angle, θ is determined in VidPro (Nugent & Iverson 2011) as:

The position angle is adjusted for drift angle and quadrant position in relation to the primary star.

The separation for each video frame, ρ in pixels is calculated as:

In the above equations [7] and [8], x_p, y_p are the

$$\theta = \arctan\left(\frac{x_p - x_s}{y_p - y_s}\right) \qquad [7]$$

primary (brighter) star coordinates, x_s, y_s – secondary star coordinates and δ is the declination of the double star.

In order to convert separation ρ from pixels to

$$\rho = \sqrt{\left(x_p - x_s\right)^2 + \left(y_p - y_s\right)^2}\ \cos\delta \qquad [8]$$

arcseconds, the scale factor *S* is calculated as:

where x_b, x_e, y_b, and y_e are the coordinates of the points at the beginning and the end of the drift for each

$$S = \frac{dt 15.041068}{\sqrt{\left(x_b - x_e\right)^2 + \left(y_b - y_e\right)^2}} \qquad [9]$$

star and *dt* is the time of drift in seconds, calculated from the 29.921 frames per second video frame rate.

The pixel scale factor and drift angle are calculated for each video drift. The average pixel scale for 10 recorded video drifts with 2x binning applied was 0.357" per pixel (standard deviation σ = 0.0039").

5. Target Selection

The selection criteria were as follows:

1. Favourable positioning in the sky within the 35° zenith angle;
2. 0.6" – 10" separation in order to compare the selected methods of measurements;
3. Dimmest star on the pair brighter than 8th visual magnitude (determined during a trial run)

18 double stars were selected for observations during 6 runs, which are listed in Table 1.

The primary and secondary visual magnitude values (m1 and m2) and spectral class data were taken from the WDS Catalog, orbit grades (O G) from the Sixth Orbit Catalog (1 – 5 numeric grade, U – Uncertain double, P – Physical binary but without orbital parameters, N – Non-physical double), SEP (in degrees) and PA (in arcseconds) were calculated ephemerides, where applicable. Exposure time in milliseconds was set based on visual magnitude values and the outcome of the test run.

6. Observation Results

Speckle Interferometry results

The results of Speckle Interferometry measurements for 18 double stars with separations ranging from 0.64" to 11.45" are presented in Table 2. The errors are discussed in Section 9.

Lucky Imaging results

It was not possible to detect centroids for stars closer than 1" with the Lucky Imaging method. Double stars with orbit grades 4 or better and separations larger than 1", measured by the Speckle Interferometry method, were also measured using Lucky Imaging method for comparison. Non-physical double 02583-4018 PZ 2 was included for comparison with the Video Drift method because of its wider separation. The results of Lucky Imaging measurements for 8 double stars are presented in Table 3.

(Text continues on page 662)

A Comparison of Methods for Astrometric Measurements of Close Double Stars

Table 1. Observation targets for six observing sessions 2017-08-30 to 2017-10-15. PA and SEP are the position angle in degrees and separation in arceseconds, calculated from orbital parameters where orbits are available or last observed values from WDS where orbits are not available. OG is the orbit grade. Spectral classes are from WDS. Exposure values in milliseconds are estimated based on previous test runs.

NAME	RA+DEC	MAGS	PA	SEP	OG	Spectral Class	Exp ms	Notes
BU 391AB	00094-2759	6.13,6.24	258.12	1.301	5	F4IV-V (yellow-white)	30	
BU 395	00373-2446	6.60,6.20	117.7	0.626	1	G8V (yellow)	30	
HDO 182	00427-3828	6.60,7.01	139.37	0.513	5	A0V (white)	30	1
I 47	00519-4343	7.45,7.95	30.65	0.603	5	F2V+F5V (yellow-white/ yellow-white)	30	
SLR 1AB	01061-4643	4.10,4.19	80.64	0.616	3	G8IIIv (yellow)	8	
DUN 5	01398-5612	5.78,5.90	186.2	11.45	4	K0V+K5V (yellow-orange/ yellow-orange)	30	2,6
STF 202AB	02020+0246	4.10,5.17	265	1.8	4	A0p+A3m (white/white)	10	
PZ 2	02583-4018	3.20,4.12	90.55	8.43	N	A4III+A1V (white/white)	4	3,6
RHD 1AB	14396-6050	-0.01,1.33	313	4.1	2	G2V+K1V (yellow/yellow-orange)	0.6	
H 2 19AB	16256-2327	5.07,5.74	338	3.2	5	B2IV+B2V (blue-white/ blue-white)	30	
SHJ 243AB	17153-2636	5.12,5.12	143	5.4	4	K5Ve+K1V (yellow-orange/ yellow-orange)	30	
HJ 5014	18068-4325	5.65,5.68	363	1.8	4	A5V+A5V (white/white)	30	
HDO 150AB	19026-2953	3.27,3.48	252	0.6	1	A2III (white)	4	
HJ 5084	19064-3704	4.53,6.42	343	1.6	2	F8V+F8V (yellow-white/ yellow-white)	30	
BU 276	22008-2827	5.70,6.77	115	1.2	U	B8Ve (blue-white)	30	4
SHJ 345AB	22266-1645	6.29,6.39	78	1.3	4	G0V+G0V (yellow/yellow)	30	
DUN 251	23395-4638	6.53,7.27	279	4.1	P	A8V+F0V (white/yellow-white)	30	5
H 2 24	23460-1841	5.65,6.46	135	7	P	A9IV+F2V (white/yellow-white)	30	6

Notes:

1. Speckle Interferometry measurements show a large error in position angle compared to ephemeris. Orbit parameters are possibly incorrect (discussed in the Error Analysis Section).
2. Orbit parameters are slightly incorrect. Using last precise measurement from 2016 listed in WDS, Sca2015c (discussed in the Error Analysis Section)
3. Non-physical double. Measurements from Anton (2010).
4. Uncertain double. Measurements from Horch et al. (2010).
5. Physical double without orbital solution. Data from int4_web, Tok2006a.
6. Separation is too large for Speckle Interferometry. Speckle measurements included for comparison with Lucky Imaging and Video Drift methods.

A Comparison of Methods for Astrometric Measurements of Close Double Stars

Table 2. Speckle Interferometry results. Observed from 37.98°S latitude, 145.06°E longitude, Melbourne, Australia with 8" Schmidt-Cassegrain telescope. "PA meas" and "SEP meas" are the measured position angle in degrees and separation in arcseconds. "D PA" and "D SEP" are the residuals between the observed and computed or last observed values. "STDEV PA" and "STDEV SEP" are the standard deviation values of multiple measurements

NAME	RA+DEC	MAGS	PA	SEP	DATE	N	D	D	STDEV	STDEV
			meas	meas			PA	SEP	PA	SEP
BU 391AB	00094-2759	6.13,6.24	258.28	1.363	2017.745	1	0.16	0.062	0.225	0.007
			258.02	1.342	2017.781	1	-0.1	0.041	0.224	0.005
BU 395	00373-2446	6.60,6.20	123.88	0.875	2017.778	1	6.18	0.249	5.269	0.03
HDO 182	00427-3828	6.60,7.01	22.64	0.753	2017.742	1	-116.73	0.24	1.41	0.027
			24	0.782	2017.745	1	-115.38	0.269	0.508	0.005
I 47	00519-4343	7.45,7.95	28.52	0.832	2017.745	1	-2.13	0.229	0.562	0.039
SLR 1AB	01061-4643	4.10,4.19	73.95	0.642	2017.658	1	-6.69	0.026	0.894	0.015
			75.8	0.681	2017.742	1	-4.84	0.065	0.517	0.015
			89.19	0.74	2017.775	1	8.87	0.121	0.47	0.002
DUN 5	01398-5612	5.78,5.90	186.55	11.446	2017.775	1	0.35	-0.004	0.041	0.007
			186.59	11.441	2017.781	1	0.39	-0.004	0.03	0.005
STF 202AB	02020+0246	4.10,5.17	263.17	1.888	2017.781	1	1.63	0.054	0.155	0.008
PZ 2	02583-4018	3.20,4.12	91.45	8.373	2017.742	1	0.35	-0.257	0.054	0.007
RHD 1AB	14396-6050	-0.01,1.33	323.98	4.341	2017.658	1	0.82	0.005	0.054	0.004
H 2 19AB	16256-2327	6.30,6.80	334.13	3.023	2017.658	1	-2.91	0.158	0.13	0.012
SHJ 243AB	17153-2636	5.12,5.12	139.97	5.103	2017.658	1	-0.05	0.046	0.105	0.004
HJ 5014	18068-4325	5.65,5.68	360.56	1.797	2017.658	1	1.68	0.058	0.209	0.004
HDO 150AB	19026-2953	3.27,3.48	220.87	0.719	2017.658	1	-25.41	0.164	3.84	0.012
HJ 5084	19064-3704	4.53,6.42	338.17	1.429	2017.658	1	0.17	-0.021	0.384	0.012
BU 276	22008-2827	5.70,6.77	113.17	1.891	2017.658	1	-1.73	0.671	0.22	0.01
			113.17	1.89	2017.742	1	-1.73	0.67	0.228	0.018
SHJ 345AB	22266-1645	6.29,6.39	72.22	1.336	2017.778	1	-0.36	0.04	0.015	0.000
			71.75	1.347	2017.781	1	-0.83	0.051	0.377	0.002
DUN 251	23395-4638	6.53,7.27	277.49	3.855	2017.745	1	-1.61	-0.205	0.052	0.003
H 2 24	23460-1841	5.65,6.46	135.15	6.993	2017.658	1	-0.05	-0.018	0.014	0.001

Table 3. Lucky Imaging results. Observed from 37.98°S latitude, 145.06°E longitude, Melbourne, Australia with 8" Schmidt-Cassegrain telescope. "PA meas" and "SEP meas" are the measured position angle in degrees and separation in arcseconds. "D PA" and "D SEP" are the residuals between the observed and computed or last observed values. "STDEV PA" and "STDEV SEP" are the standard deviation values of multiple measurements

NAME	RA+DEC	MAGS	PA meas	SEP meas	DATE	N	D PA	D SEP	STDEV PA	STDEV SEP
BU 391AB	00094-2759	6.13,6.24	257.54	1.331	2017.745	1	-0.58	0.03	0.302	0.012
			258.43	1.34	2017.781	1	0.31	0.039	0.775	0.037
DUN 5	01398-5612	5.78,5.90	186.58	11.439	2017.775	1	0.03	-0.011	0.052	0.01
			186.51	11.448	2017.781	1	-0.05	-0.002	0.082	0.008
STF 202AB	02020+0246	4.10,5.17	264.32	1.781	2017.781	1	2.78	-0.053	1.118	0.083
PZ 2	02583-4018	3.20,4.12	91.44	8.376	2017.658	1	0.34	-0.254	0.069	0.009
RHD 1AB	14396-6050	-0.01,1.33	324.03	4.33	2017.658	1	0.87	-0.006	0.128	0.013
SHJ 243AB	17153-2636	5.12,5.12	140.11	5.102	2017.658	1	0.09	0.045	0.179	0.017
HJ 5014	18068-4325	5.68,5.68	360.37	1.765	2017.658	1	1.49	0.026	0.237	0.015
HJ 5084	19064-3704	4.53,6.42	338.83	1.46	2017.658	1	0.83	0.01	0.667	0.011

(Continued from page 659)

Video Drift Results

It was not possible to track double star positions with separations smaller than 4" in Tangra, due to overlapping point spread function fitting circles. Therefore, only 5 wider double stars were measured with the Video Drift method and the results are presented in Table 4.

7. Error Analysis

Speckle Interferometry errors

Overall 25 observations were made during six observing runs with the observed separations ranging from 0.64" to 11.5". 18 measurements of double stars wider than 1", produced reliable results with the Speckle Interferometry method. The average absolute separation O-C residual was 0.04" and the average absolute position angle O-C residual – 0.52º.

Six measurements of binary stars closer than 1" were less reliable – the average absolute O-C separation residual was 0.142" and average absolute O-C position angle residual was 9.02º. Two measurements of 00427-3828 HDO 182 were excluded from the statistical analysis due to suspected errors in the orbital parameters provided in the Sixth Orbit Catalog (discussed below).

Separation and position angle residuals plotted against separation (Figures 9, 10) show that separations of double stars closer than 0.6" are overestimated and position angles have larger errors. Considering that 0.6" is below the telescopes resolution limit (0.7", according

Table 4. Video Drift results. Observed from 37.98°S latitude, 145.06°E longitude, Melbourne, Australia with 8" Schmidt -Cassegrain telescope. "PA meas" and "SEP meas" are the measured position angle in degrees and separation in arcseconds. "D PA" and "D SEP" are the residuals between the observed and computed or last observed values. "STDEV PA" and "STDEV SEP" are the standard deviation values of multiple measurements.

NAME	RA+DEC	MAGS	PA meas	SEP meas	DATE	N	D PA	D SEP	STDEV PA	STDEV SEP
DUN 5	01398-5612	5.78,5.90	186.46	11.34	2017.658	1	0.25	-0.11	1	0.16
			186.51	11.34	2017.658	1	0.31	-0.11	0.905	0.105
PZ 2	02583-4018	3.20,4.12	90.07	8.325	2017.658	1	-1.03	-0.305	0.735	0.13
RHD 1AB	14396-6050	-0.01,1.33	324.34	4.243	2017.742	1	1.18	-0.093	2.11	0.153
SHJ 243AB	17153-2636	5.12,5.12	140.05	5.05	2017.775	1	0.03	-0.007	1.02	0.12
H 2 24	23460-1841	5.65,6.46	134.69	7.011	2017.658	1	-0.51	-0.014	0.728	0.095

to the Rayleigh criterion) such results are expected and these measurements were done out of curiosity to see how close the little 8-inch Celestron telescope can go.

These plots also show that negative and positive residuals are distributed reasonably evenly and there are no significant systematic errors in the measurements, other than the expected over-estimation of separation for very close doubles (1" or less)

Two residuals (compared with the original catalogue values), however stood out and prompted further investigations.

1. 00427-3828 HDO 182 (λ Scl)

The ephemeris for λ Scl predicts the position angle 139.37º and separation 0.513" but average measured values from two runs on different nights were 23.32º and 0.76" , respectively.

Further investigation suggests that the Grade 5 orbit in the Sixths Orbit Catalog is incorrect and may need adjustment. Fourth Catalog of Interferometric Measurements of Binary Stars (int4_web) contains 12 measurements of λ Scl with the position angle slowly increasing from 13.7º to 17.5º from 1989 to 1996. Two last measurements in 2008 by Tokovinin however, record the position angle of 199.6º; and are likely to be erroneous (perhaps a misplaced decimal point). Anton (2010) observed λ Scl in 2008 with 0.4m telescope using Lucky Imaging method and recorded the position angle of 21º.

Considering these errors, λ Scl was excluded from the statistical analysis.

2. 01398-5612 DUN 5 (p Eri)

The ephemeris for p Eri predicts the position angle 186.34º and separation 11.62", but average measured values from two runs on different nights were 186.57º and 11.4". The separation residual of 0.181 is too large compared with all other Speckle Interferometry residuals.

The measurements with Lucky Imaging and Video Drift methods showed results consistent with the values obtained with Speckle Interferometry method. Therefore, the last precise position measurement from 2016 (186.2º and 11.4") listed in the WDS Catalog was used as a reference instead.

Lucky imaging errors

7 binary stars with orbit grades 4 or better and one non-physical double star were measured using Lucky imaging method with 10 total measurements. The average absolute separation residual was 0.03" and the average absolute position angle residual was 0.90º.

Separation and position angle residuals plotted against separation (Figures 11, 12) show that the errors are comparable with the Speckle Interferometry method and there were no obvious systematic errors in measurements using Lucky Imaging method.

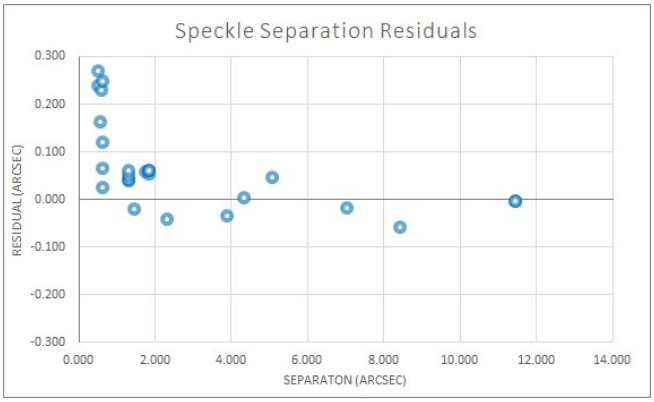

Figure 9. Speckle Interferometry – Separation O-C residuals vs Separation.

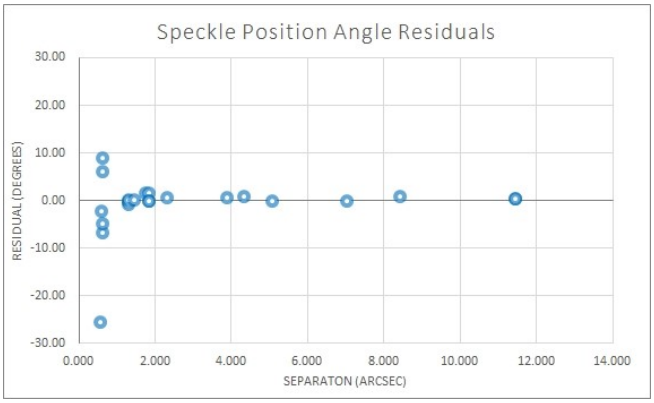

Figure 10. Speckle Interferometry – Position Angle O-C residuals vs Separation

Figure 11. Lucky Imaging – Separation O-C residuals vs Separation.

4 binary stars with orbit grades 4 or better and one non-physical double star were measured using Lucky imaging method with 6 total measurements (Figures 13, 14). The average absolute separation residual was 0.06" and the average absolute position angle residual – 0.46º.

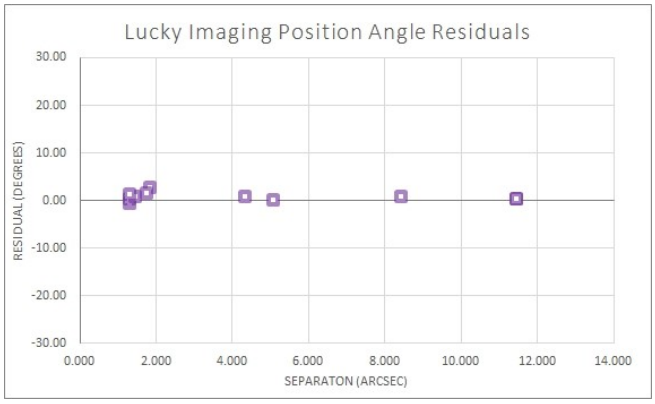

Figure 12. Lucky Imaging – Position Angle O-C residuals vs Separation

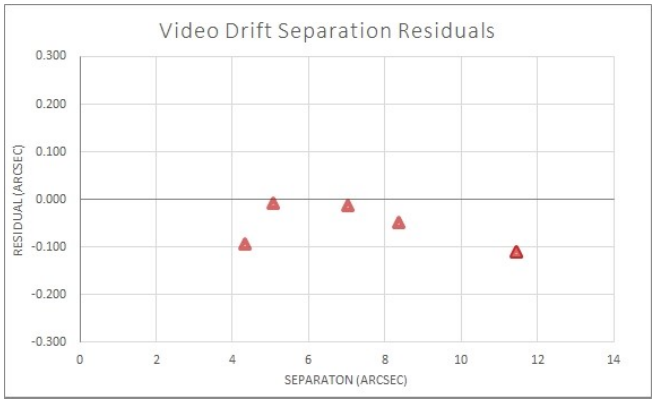

Figure 13. Video Drift – Separation O-C residuals vs Separation.

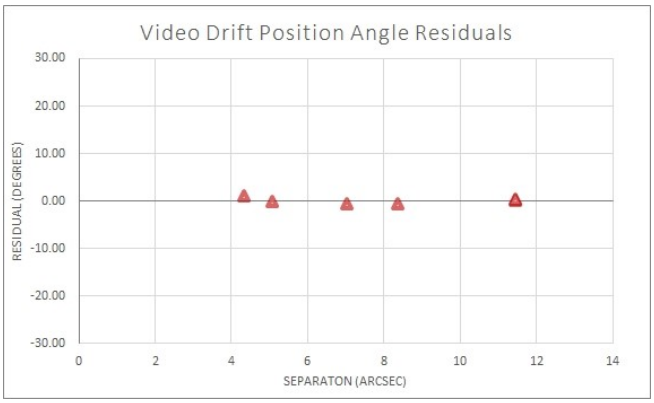

Figure 14. Video Drift – Position Angle O-C residuals vs Separation

8. Comparison of Methods

Figure 15 shows the data reduction results for RHD 1AB (Alpha Centauri, separation 4.33") using three methods:

- Lucky — the stack of 117 best frames.
- Speckle — the autocorrelogram, ready to be measured.
- Video Drift — the sum of 330 video frames without tracking. The speckle pattern is clearly visible.

The O-C residuals, computed from the Sixth Orbit Catalogue ephemerides (or last precise observations for those without orbits), were converted from polar to rectangular coordinates and plotted in Figure 16 in order to assess and compare the precision of measurements. Double stars closer than 1" were excluded from the plot because they could only be measured with the Speckle Interferometry method and the uncertainty of measurements was too large.

It is evident from the result tables and the plot, that Video Drift method produced the least accurate results with a tendency to under-estimate the separation parameters. Speckle Interferometry and Lucky Imaging methods produced results with similar accuracy, and all of the residuals were well within the one-pixel square, represented by the dotted line on the plot.

The results are summarized in Table 5

From the practical point of view, the easiest method to apply during image acquisition is the Video Drift Method, as it does not require tracking and no additional steps to determine image scale and angle. Image acquisition for the Speckle Interferometry and Lucky Imaging methods is identical and can be somewhat laborious, due the difficulties in pointing a consumer grade telescope mount with the sufficient precision, consider-

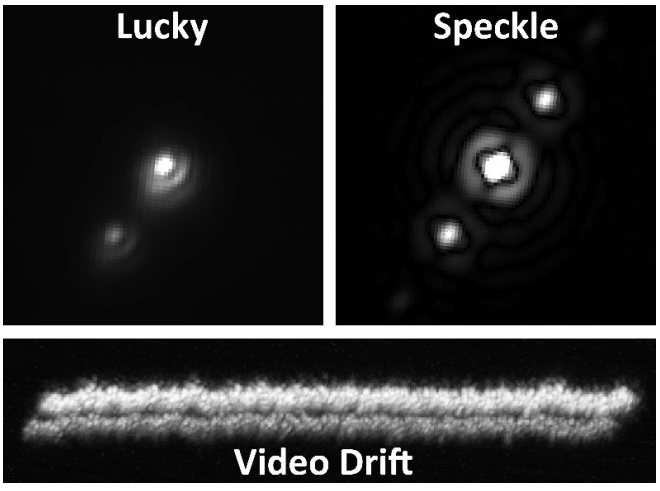

Figure 15. Data reduction of RHD 1AB (Alpha Centauri) using three methods.

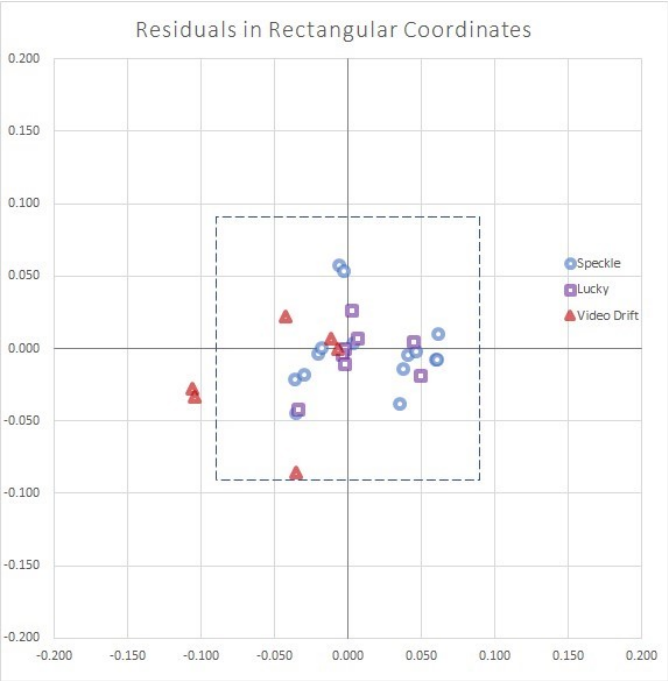

Figure 16. O-C residuals plotted in rectangular coordinates for measurements obtained with different methods. Blue circles represent Speckle Interferometry, purple rectangles – Lucky Imaging and red triangles – Video Drift results. The dash-lined square represents one pixel in the instrumental setup.

ing a very narrow field of view. Use of the full 36x24mm frame in Canon 6D camera with the Open Source Magic Lantern software for that purpose was definitely helpful. Alternatively, a second, shorter telescope can be coupled with the main instrument and used for pointing, but it requires additional hardware.

The data reduction process was the easiest and quickest with the Speckle Toolbox, thanks to semi-automated method of reduction, which after preparation of a text input file required least manual steps and waiting time to obtain the results. It was also rather difficult to measure doubles closer than 3" using Lucky imaging.

9. Conclusions

Successful series of double star observations were performed in the field using a small consumer-grade telescope and a DSLR camera. Data reduction was performed using three different methods and near diffraction-limited results were obtained using Speckle Interferometry and Lucky Imaging methods.

The Video Drift method is well suited for observations of wider pairs, separated by more than 4". It does not require reference stars and calculates image scale and orientation from the drift data automatically. This method would be most appealing to the owners of

Table 5. Summary of the results for pairs wider than 1". NS is the number of measured doubles Min SEP— minimum separation measured with the particular method; O-C PA, O-C SEP — average absolute Observed — Computed residuals; STDEV O-C PA, STDEV O-C SEP — standard deviation values for O-C residuals in Position Angle and Separation

METHOD	NS	Min SEP	O-C PA	STDEV O-C PA	O-C SEP	STDEV O-C SEP
Speckle	18	1.3	0.52	0.15	0.04	0.01
Lucky	8	1.3	0.90	0.38	0.03	0.02
Video Drift	5	4.3	0.46	1.08	0.06	0.13

"Dobsonian" telescopes and is quite easy to use.

Lucky Imaging and Speckle Interferometry allow us to measure double stars close to the telescope's resolution limit. Although the learning curve for the data reduction and analysis is steeper than with the Video Drift, the availability of well documented Speckle Toolbox and REDUC software programs makes it an enjoyable process. Overall, the measurements in Speckle Toolbox are more precise and repeatable, especially at smaller separations. The U. S. Naval Observatory uses speckle-style data reduction for even wider pairs, even when there is no isoplanicity or interference, because this method provides more precise measurements than Lucky Imaging (Harshaw et al. 2017).

Antoine Labeyrie (1970) in his pioneering paper on Speckle Interferometry concluded that it is capable of achieving 0.02" resolution but requires "the largest possible telescope and sensitive image receivers such as image intensifiers or electronographic cameras". Advances in computing bring the Speckle Interferometry method to personal computers and modern digital cameras make it available to most amateur astronomers, even with very small telescopes, by professional standards.

10. Images

The reduction process involves processing of large number of images and the working folder at the conclusion of this project contains 577,000 image and text files, with the total size of 1.2 Terabytes. Subsets of RAW videos, FITS images and FITS cubes are available upon request.

11. Acknowledgements

This research project was done as part of Swinburne Astronomy Online postgraduate program and special thanks are extended to Swinburne University of Technology and Eduardo Alvarez for the opportunity and guidance in working on the project.

Warm thanks are extended to David Rowe, Florent

Losse, Richard Nugent and Hristo Pavlov for developing and maintaining excellent free software which made this research project possible.

This research has made use of the Washington Double Star Catalog maintained at the U.S. Naval Observatory.

12. References

Double Stars, Heintz, W.D., Dordrecht, D. Reidel Publishing Co 1978.

Observing and Measuring Visual Double Stars, 2nd edition, B. Argyle, Springer-Verlag London 2012.

Boffin H., Hussain, G., Berger, J.P. & Schmidtobreick, L. 2016, *Astronomy at High Angular Resolution* (Springer International Publishing Switzerland).

Genet, R.M., Ridgely, J., Teiche, A., Foley, E., Christiansen, C., Rowe, D., Zimmerman, N., Knox, K., Hege, K., Kenney, J., *et al.*, 2015, "Speckle Interferometry of Short-Period Binary Stars", *Journal of Double Star Observations,* **11**, 151.

Harshaw, R., Rowe, D. and Genet, R., 2017, "The Speckle Toolbox: A Powerful Data Reduction Tool for CCD Astrometry*", Journal of Double Star Observations*, **13**, 52-67.

Horch, E., Franz, O.G. and Ninkov, Z., 2000, "CCD speckle observations of binary stars from the southern hemisphere. II. Measures from the Lowell-Tololo telescope during 1999", *The Astronomical Journal,* **120**, 2638.

Labeyrie, A., 1970, "Attainment of diffraction limited resolution in large telescopes by Fourier analysing speckle patterns in star images", *Astron. Astrophys*, **6**, 85-87.

Michell, J., 1767, "An inquiry into the probable parallax and magnitude of the Fixed Stars, etc.", *Phil. Trans.*, **57**, 234.

Nugent, R. and Iverson, E.W., 2010, "A New Video Method to Measure Double Stars", *Journal of Double Star Observations*, 2011, **7**, 185-194.

Rutkowski, A. and Waniak, W., 2005, "Speckle observations of binary stars with a 0.5 m telescope", *Publications of the Astronomical Society of the Pacific*, **117**, 1362.

Sofieva, V.F., Dalaudier, F. and Vernin, J., 2013, "Using stellar scintillation for studies of turbulence in the Earth's atmosphere", *Phil. Trans. R. Soc.* A, 371 .

Tokovinin, A., Mason, B.D. and Hartkopf, W.I., 2010, "Speckle Interferometry at the Blanco and SOAR Telescopes in 2008 and 2009", *The Astronomical Journal*, **139**, 743.

astroplanner_web: AstroPlanner, http://astroplanner.net/ (accessed 24 March 2018)

int4_web: Fourth Catalog of Interferometric Measurements of Binary Stars, http://www.usno.navy.mil/USNO/astrometry/optical-IR-prod/wds/int4/fourth-catalog-of-interferometric-measurements-of-binary-stars (accessed 24 March 2018)

mlvmystic_web: MLVMystic, https://github.com/GTempler/MLVMystic (accessed 24 March 2018)

planewave_web: Software and Update, http://planewave.com/downloads/software/ (accessed 24 March 2018)

reduc_web: REDUC, http://www.astrosurf.com/hfosaf/reduc/tutorial.htm (accessed 24 March 2018)

sgpro_web: Sequence Generator Pro v2.6, http://mainsequencesoftware.com/Products/SGPro (accessed 24 March 2018)

tangra_web: Tangra, http://www.hristopavlov.net/Tangra3/ (accessed 24 March 2018)

wds_web: Washington Double Star Catalogue, http://ad.usno.navy.mil/wds/ (accessed 24 March 2018)